Decision–Feedback Differential Detection of MDPSK for Flat Rayleigh Fading Channels

Robert Schober, *Student Member, IEEE*, Wolfgang H. Gerstacker, *Student Member, IEEE*, and Johannes B. Huber, *Member, IEEE*

Abstract

In this paper, decision–feedback differential detection (DF–DD) of M–ary differential phase–shift keying (MDPSK) signals, which has been introduced previously for the additive white Gaussian noise (AWGN) channel by Leib et al. [1] and Edbauer [2], is extended to flat Rayleigh fading channels. The corresponding DF–DD metric is derived from the multiple–symbol detection (MSD) metric and for genie–aided DF–DD an exact expression for the bit error rate (BER) of QDPSK ($M = 4$) is calculated. Furthermore, the dependence of BER on the power spectrum of the fading process is investigated for feedback filters of infinite order. It is shown that in this case, for ideally bandlimited fading processes the error floor of conventional differential detection (DD) can be removed entirely. Simulation results confirm that both, MSD and DF–DD with feedback filters of finite order can reduce the error floor of conventional DD significantly. Thereby, DF–DD causes considerably less computational load.

Index Terms–Differential detection, M–ary DPSK, Rayleigh channels, flat fading, decision–feedback.

1 Introduction

It is well known, that differential detection (DD) of M–ary differential phase–shift keying (MDPSK) is attractive for flat fading environments since it is very robust and does not require carrier phase tracking. However, performance of conventional DD in flat fading channels is limited by an error floor if the fading bandwidth B_f is larger than zero, i.e., if the autocorrelation function of the fading process is not a constant [3]. Divsalar et al. have introduced multiple–symbol detection (MSD) of MDPSK signals transmitted over the additive white Gaussian noise (AWGN) channel [4]. The same authors [5] and Ho et al. [6] have extended MSD to fading channels. The main disadvantage of MSD is its high complexity. For the AWGN channel, Leib et al. [1] and Edbauer [2] proposed simple decision–feedback differential detection (DF–DD) techniques which provide a good performance at a very low computational complexity. Adachi et al. showed in [7] that these schemes are identical and can be derived from MSD by introducing decision–feedback symbols into the MSD metric. Motivated by this result we extend DF–DD to Rayleigh fading channels. It will be shown that for such channels, DF–DD is a very effective method to reduce the error floor of conventional DD. In contrast to other detection schemes proposed for Rayleigh fading (see e.g. [8, 9, 10, 11]) our technique does not apply oversampling or sequence estimation.

The paper is organized as follows. In Section 2, the transmission model is presented and in Section 3 the metric of DF–DD for Rayleigh fading channels is derived. In Section 4, the bit error rate (BER) of QDPSK ($M = 4$) for genie–aided DF-DD is calculated and in Section 5, the relation of DF–DD to linear prediction is investigated and an alternative expression for BER is given. Then, in Section 6 the limiting performance of the receiver for an infinite number of feedback symbols is discussed. Simulation results are given in Section 7 and some conclusions are drawn in Section 8.

2 Transmission Model

Fig. 1 shows a block diagram of the transmission model under consideration. For simplicity, all signals are represented by their complex–valued baseband equivalents. The MDPSK symbols are denoted by $a[k] \in \mathcal{A}_\phi \triangleq \{e^{j(\frac{2\pi\nu}{M}+\phi)} | \nu \in \{0, 1, \ldots, M-1\}\}$, $\phi \in$

$\{0, \frac{\pi}{M}\}$, and the corresponding differentially encoded MPSK symbols $b[k]$ are given by

$$b[k] = a[k]b[k-1], \qquad k \in \mathbb{Z}. \tag{1}$$

Both, transmitter filter $H_t(f)$ and receiver filter $H_r(f)$, have square–root Nyquist characteristic. Hence, no intersymbol interference occurs as long as the time–continuous fading process $f_c(t)$ with equivalent one–sided bandwidth B_f does not change significantly during the symbol interval T. In this paper, we assume that this condition is fulfilled for $B_f T \leq 0.03$. Thus, we assume that the samples $r[k]$ of the received signal $r(t)$ can be written as

$$r[k] = r(kT) = f[k]b[k] + n[k], \tag{2}$$

where the fading process $f[\cdot]$ and the noise process $n[\cdot]$ are correlated and uncorrelated zero mean complex Gaussian random processes, respectively. Furthermore, $n[\cdot]$ and $f[\cdot]$ are assumed to be mutually uncorrelated. Due to an appropriate normalization, $f[k]$ and $n[k]$ have variance $\sigma_f^2 = \mathcal{E}\{|f[k]|^2\} = 1$ and $\sigma_n^2 = \mathcal{E}\{|n[k]|^2\} = \frac{N_0}{E_s}$. Here, $\mathcal{E}\{\cdot\}$ denotes expectation and E_s is the mean received energy per symbol, whereas N_0 is the one–sided power spectral density of the underlying passband noise process. At the receiver, the estimated symbols $\hat{a}[k]$ are determined by DF–DD.

3 Derivation of the DF–DD Metric for Rayleigh Fading Channels

In this section, the DF–DD metric for Rayleigh fading channels is derived. Since the proposed DF–DD metric is based on the optimum MSD metric, we first consider MSD. For MSD, observation intervals of length NT, $N > 1$, have to be introduced and the vector $\boldsymbol{r}_k \triangleq [r[k], r[k-1], \ldots, r[k-N+1]]^T$, where $[\cdot]^T$ denotes the transpose of a vector, may be written in the form

$$\boldsymbol{r}_k = \boldsymbol{B}_k \boldsymbol{f}_k + \boldsymbol{n}_k, \tag{3}$$

where the definitions

$$\boldsymbol{B}_k \triangleq \mathrm{diag}\{b[k], b[k-1], \ldots, b[k-N+1]\}, \tag{4}$$

$$\boldsymbol{n}_k \triangleq [n[k], n[k-1], \ldots, n[k-N+1]]^T, \tag{5}$$

$$\boldsymbol{f}_k \triangleq [f[k], f[k-1], \ldots, f[k-N+1]]^T, \tag{6}$$

are used. Here, the notation $\mathrm{diag}\{x_1, x_2, \ldots, x_L\}$ stands for an $L \times L$ diagonal matrix with diagonal elements x_ν, $1 \leq \nu \leq L$. Since $\boldsymbol{r}_k$ is the sum of two zero mean Gaussian random vector processes, the conditional probability density function (pdf) $p(\boldsymbol{r}_k|\boldsymbol{a}_k)$ of $\boldsymbol{r}_k$ for the transmitted symbol vector $\boldsymbol{a}_k \triangleq [a[k], a[k-1], \ldots, a[k-N+2]]^T$ is [9, 12]

$$p(\boldsymbol{r}_k|\boldsymbol{a}_k) = \frac{1}{\pi^N |\boldsymbol{R}_a|} \mathrm{e}^{-\boldsymbol{r}_k^H \boldsymbol{R}_a^{-1} \boldsymbol{r}_k}, \tag{7}$$

where $[\cdot]^H$ and $|\cdot|$ denote the Hermitian transpose and the determinant of a matrix, respectively, and $\boldsymbol{R}_a$ is the $N \times N$ (conditional) autocorrelation matrix of $\boldsymbol{r}_k$

$$\boldsymbol{R}_a = \mathcal{E}\{\boldsymbol{r}_k \boldsymbol{r}_k^H | \boldsymbol{a}_k\}. \tag{8}$$

Using the notation

$$\boldsymbol{R}_f \triangleq \mathcal{E}\{\boldsymbol{f}_k \boldsymbol{f}_k^H\}, \tag{9}$$

$\boldsymbol{R}_a$ can be written as

$$\boldsymbol{R}_a = \boldsymbol{B}_k \boldsymbol{R}_f \boldsymbol{B}_k^H + \sigma_n^2 \boldsymbol{I}, \tag{10}$$

where $\boldsymbol{I}$ is the $N \times N$ identity matrix. Note, that $p(\boldsymbol{r}_k|\boldsymbol{a}_k)$ does not depend on the absolute phase of $\boldsymbol{b}_k \triangleq [b[k], b[k-1], \ldots, b[k-N+1]]^T$, cf. Eqs. (7), (10). Thus, by exploiting Eq. (7) it is only possible to decide upon $\boldsymbol{a}_k$ but not upon $\boldsymbol{b}_k$. The maximum–likelihood decision for $\boldsymbol{a}_k$ corresponding to MSD can be obtained by maximizing $p(\boldsymbol{r}_k|\boldsymbol{a}_k)$. This is equivalent to the maximization of the metric

$$\eta = -\boldsymbol{r}_k^H \boldsymbol{R}_a^{-1} \boldsymbol{r}_k - \ln |\boldsymbol{R}_a|. \tag{11}$$

Note, that the same result was derived in [5] and [6][1]. In contrast to [5] and [6], we transform the metric of Eq. (11) into a simpler form and use it for derivation of the DF–DD metric. Because of the relation $\boldsymbol{B}_k \boldsymbol{B}_k^H = \boldsymbol{I}$, $\boldsymbol{R}_a$ can be expressed as

$$\boldsymbol{R}_a = \boldsymbol{B}_k (\boldsymbol{R}_f + \sigma_n^2 \boldsymbol{I}) \boldsymbol{B}_k^H \triangleq \boldsymbol{B}_k \boldsymbol{R} \boldsymbol{B}_k^H. \tag{12}$$

Thus, the determinant of $\boldsymbol{R}_a$ may be rewritten as

$$|\boldsymbol{R}_a| = |\boldsymbol{B}_k||\boldsymbol{R}||\boldsymbol{B}_k^H| = |\boldsymbol{B}_k||\boldsymbol{R}||\boldsymbol{B}_k|^H = |\boldsymbol{R}|, \tag{13}$$

[1] The metric in [5] and [6] is $\eta = -\frac{1}{2}\boldsymbol{r}_k^H \boldsymbol{R}_a^{-1} \boldsymbol{r}_k - \ln |\boldsymbol{R}_a|$. A comparison with Eq. (11) shows that there is an additional factor $\frac{1}{2}$. This is due to the different definition of expectation used in [5] and [6]. There $\boldsymbol{R}_a \triangleq \frac{1}{2}\mathcal{E}\{\boldsymbol{r}_k \boldsymbol{r}_k^H | \boldsymbol{a}_k\}$ is used, whereas we use the definition according to Eq. (8).

and therefore is independent of the transmitted symbol sequence. Using this in addition to Eq. (12) and $\boldsymbol{B}_k^H = \boldsymbol{B}_k^{-1}$, the MSD metric of Eq. (11) can be simplified to

$$\eta' = -\boldsymbol{r}_k^H \boldsymbol{B}_k \boldsymbol{R}^{-1} \boldsymbol{B}_k^H \boldsymbol{r}_k. \tag{14}$$

Since the negative correlation matrix $-\boldsymbol{R}$ is Hermitian, its inverse $\boldsymbol{T}$ has the same property [13]. Thus, it is possible to express $\boldsymbol{T}$ by

$$\boldsymbol{T} = -\boldsymbol{R}^{-1} \triangleq \begin{bmatrix} t_{0\,0} & t_{0\,1} & \dots & \dots & t_{0\,N-1} \\ t_{1\,0} & t_{1\,1} & t_{1\,2} & \dots & \vdots \\ \vdots & \ddots & \ddots & \ddots & \vdots \\ t_{N-2\,0} & \ddots & \ddots & t_{N-2\,N-2} & t_{N-2\,N-1} \\ t_{N-1\,0} & \dots & \ddots & t_{N-1\,N-2} & t_{N-1\,N-1} \end{bmatrix}, \tag{15}$$

where $t_{\nu\,\mu} = t_{\mu\,\nu}^*$ holds for $0 \leq \nu, \mu \leq N-1$ ($(\cdot)^*$ denotes complex conjugation). By applying Eq. (15), Eq. (14) can be rewritten as

$$\begin{aligned} \eta' &= \sum_{\nu=0}^{N-1} \sum_{\mu=0}^{N-1} t_{\nu\,\mu} b[k-\nu] b^*[k-\mu] r^*[k-\nu] r[k-\mu] \\ &= \sum_{\nu=0}^{N-1} t_{\nu\,\nu} |b[k-\nu]|^2 |r[k-\nu]|^2 \\ &\quad + 2\mathrm{Re}\left\{ \sum_{\nu=0}^{N-1} \sum_{\mu=\nu+1}^{N-1} t_{\nu\,\mu} r[k-\mu] r^*[k-\nu] \prod_{j=\nu}^{\mu-1} a[k-j] \right\}, \end{aligned} \tag{16}$$

where Eq. (1) has been used. Since the result of the first sum in Eq. (16) is common to all transmitted symbol vectors $\boldsymbol{a}_k$, the estimated symbol vector $\hat{\boldsymbol{a}}_k \triangleq [\hat{a}[k],\, \hat{a}[k-1],\, \dots,\, \hat{a}[k-N+2]]^T$, $\hat{a}[\cdot] \in \mathcal{A}_\phi$, is determined by

$$\hat{\boldsymbol{a}}_k = \underset{\tilde{\boldsymbol{a}}_k}{\mathrm{argmax}} \left\{ \mathrm{Re}\left\{ \sum_{\nu=0}^{N-1} \sum_{\mu=\nu+1}^{N-1} t_{\nu\,\mu} r[k-\mu] r^*[k-\nu] \prod_{j=\nu}^{\mu-1} \tilde{a}[k-j] \right\} \right\}, \tag{17}$$

where in comparison to Eq. (16) the vector $\boldsymbol{a}_k$ of unknown transmitted symbols is replaced by the vector of trial symbols $\tilde{\boldsymbol{a}}_k \triangleq [\tilde{a}[k],\, \tilde{a}[k-1],\, \dots, \tilde{a}[k-N+2]]^T$, $\tilde{a}[\cdot] \in \mathcal{A}_\phi$ and $\hat{\boldsymbol{x}} = \underset{\tilde{\boldsymbol{x}}}{\mathrm{argmax}} \{y(\tilde{\boldsymbol{x}})\}$ denotes the vector $\tilde{\boldsymbol{x}} = \hat{\boldsymbol{x}}$ that maximizes $y(\tilde{\boldsymbol{x}})$. For determination of $\hat{\boldsymbol{a}}_k$ it is necessary to calculate M^{N-1} metrics. This corresponds to $M^{N-1}/(N-1)$ metric calculations per symbol decision, i.e., computational complexity grows exponentially with N. Although these metric calculations can be considerably simplified by using an

algorithm developed by Mackenthun [18] (see also [19], Chapter 7), a simpler and more efficient way to reduce complexity is to insert decision–feedback symbols $\hat{a}[k-\nu]$ instead of trial symbols $\tilde{a}[k-\nu]$ in Eq. (17) for all but the kth symbol $\tilde{a}[k]$, i.e., for $1 \leq \nu \leq N-2$. Thereby, instead of block decisions, symbol–by–symbol decisions result. Doing this, and omitting all summands which depend exclusively on decision–feedback symbols and thus do not influence the decision, Eq. (17) may be transformed by some straightforward manipulations into

$$\hat{a}[k] = \underset{\tilde{a}[k]}{\operatorname{argmax}} \left\{ \operatorname{Re} \left\{ \tilde{a}^*[k] r[k] \left(\sum_{\nu=1}^{N-1} t_{0\nu} r[k-\nu] \prod_{j=1}^{\nu-1} \hat{a}[k-j] \right)^* \right\} \right\}, \tag{18}$$

which is the DF–DD decision rule. Note, that as stated above a decision is now made only upon one single symbol. For simplicity, in the following we use the notation $t_\nu \triangleq t_{0\nu}$, $0 \leq \nu \leq N-1$.

If the normalized fading bandwidth $B_f T$ is zero, the autocorrelation function (ACF) of the fading process is $R_f[\lambda] \triangleq \mathcal{E}\{f[k+\lambda] f^*[k]\} = \sigma_f^2 = 1$, $\forall \lambda$. It can be shown easily from Eqs. (12) and (15) that in this case, for a given σ_n^2, $t_\nu = t_\mu$ holds for $1 \leq \nu, \mu \leq N-1$. This means, that for DF–DD, the decision rules for Rayleigh fading with $B_f T = 0$ and for AWGN are identical (cf. Eq. (11) of [1] or Eq. (12) of [2]). For $B_f T > 0$, however, $R_f[\lambda]$ is not constant $\forall\, \lambda$ and thus, in general, $t_\nu \neq t_\mu$ for $\nu \neq \mu$, $1 \leq \nu, \mu \leq N-1$, and hence, the DF–DD metric for Rayleigh fading is different from that for AWGN. Fig. 2 illustrates the behaviour of the conveniently normalized DF–DD metric coefficients $p_\nu = \sigma_e^2 t_\nu$, $1 \leq \nu \leq N-1$, for $N = 3$ and $N = 4$. The meaning of p_ν and σ_e^2 will be explained in Section 5[2]. Here, a QDPSK ($M = 4$) constellation, i.e., $\sigma_n^2 = \frac{N_0}{2E_b}$ (E_b is the mean received energy per bit), and Jakes fading model [14], i.e.,

$$R_f[\lambda] = \sigma_f^2 \mathrm{J}_0(2\pi B_f T \lambda), \quad \forall \lambda, \tag{19}$$

are assumed; $\mathrm{J}_0(\cdot)$ denotes the zeroth order Bessel function of the first kind. Fig. 2a) shows that for $B_f T = 0.0075$, $t_\nu \approx t_\mu$, $\nu \neq \mu$, $1 \leq \nu, \mu \leq N-1$, holds only at low E_b/N_0 ratios, where the channel noise is the performance limiting factor. Fig. 2b) indicates that for $B_f T = 0$, $t_\nu = t_\mu$, $1 \leq \nu, \mu \leq N-1$, for a given E_b/N_0 ratio.

[2] Note, that all t_ν, $1 \leq \nu \leq N-1$, are multiplied by the same real factor σ_e^2, whose magnitude is not of interest in this section.

Another interesting special case is $N = 2$ and $t_{01} = t_1 \in \mathbb{R}$. Here, both, MSD and DF–DD are equivalent to conventional DD for arbitrary fading bandwidths as can be seen from Eqs. (17) and (18).

Eq. (18) allows a further simplification of the decision rule. The complex plane may be divided into M sectors and then $\hat{a}[k]$ is determined uniquely by the sector into which the complex number

$$g[k] \triangleq r[k] \left(\sum_{\nu=1}^{N-1} t_\nu r[k-\nu] \prod_{j=1}^{\nu-1} \hat{a}[k-j] \right)^* \tag{20}$$

falls. This means, instead of computing $M^{N-1}/(N-1)$ MSD metrics, we only have to calculate a single complex number, namely $g[k]$. The corresponding structure is shown in Fig. 3, where the coefficients of the applied FIR feedback filter are given by the metric coefficients t_ν, $1 \leq \nu \leq N-1$.

It is worth mentioning that the DF–DD scheme presented here could be easily extended to Ricean fading. For this, the MSD metric according to Eq. (5) of [5] has to be used as starting point instead of the metric according to Eq. (11) of this paper. For derivation of the DF–DD metric again the trial symbols $\tilde{a}[k-\nu]$, $1 \leq \nu \leq N-1$, have to be replaced by feedback symbols $\hat{a}[k-\nu]$, $1 \leq \nu \leq N-1$. However, the resulting metric is more complicated than that for Rayleigh fading and it is not possible to derive a simple feedback filter structure. Thus, a closed–form performance analysis for the DF–DD metric for Ricean fading seems to be not feasable. Therefore, we restrict ourselves to the Rayleigh fading case.

4 BER of QDPSK for Genie–Aided DF–DD

In this section, we derive an expression for the BER for genie–aided DF–DD (i.e., it is assumed that all feedback symbols are correct) of QDPSK ($M = 4$). For this case, closed–form results can be obtained; furthermore, it applies to many existing systems, like the United States Digital Cellular (IS–54, IS–136) and the Japanese Digital Cellular (PDC) [15]. In order to simplify the derivation of BER, $\phi = \pi/M = \pi/4$ is assumed. Note, that amplifier nonlinearities are not taken into account and thus, the BERs for $\phi = \pi/4$ and $\phi = 0$ are the same. Our analysis follows essentially [2], however, here a Rayleigh fading channel is considered instead of an AWGN channel.

Since the BER does not depend on the transmitted symbol, it is assumed without loss of generality that $a[k] = \mathrm{e}^{j\pi/4}$ is transmitted. In this case, no symbol error occurs if the decision variable $g[k]$ (cf. Eq. (20)) falls into the 1st quadrant. The probability that $g[k]$ is located in the 2nd, 3rd and 4th quadrant is denoted by P_2, P_3 and P_4, respectively. For Gray mapping only one bit error occurs if $g[k]$ falls into the 2nd or 4th quadrant and, in addition, $P_2 = P_4$ because of symmetry. If $g[k]$ falls into the 3rd quadrant, two bit errors occur. Thus, the BER is given by

$$P_b = \frac{1}{2}(P_2 + P_4) + P_3 = P_2 + P_3. \tag{21}$$

This corresponds to

$$P_b = \Pr\{\mathrm{Re}\{g[k]\} < 0\} = \Pr\{d[k] < 0\}, \tag{22}$$

where

$$d[k] \triangleq g[k] + g^*[k] \triangleq Cx[k]y^*[k] + C^*x^*[k]y[k] \tag{23}$$

is a special case of the quadratic form of Eq. (4B.1) of [16]. By using Eqs. (1) and (2), Eq. (20) may be rewritten as

$$g[k] \triangleq a[k](f[k] + b^*[k]n[k]) \left(\sum_{\nu=1}^{N-1} t_\nu (f[k-\nu] + b^*[k-\nu]n[k-\nu]) \right)^*, \tag{24}$$

where because of the assumption of genie–aiding, $\hat{a}[k-\nu] = a[k-\nu]$, $1 \leq \nu \leq N-2$, has been used. A comparison of Eqs. (23) and (24) shows that C, $x[k]$ and $y[k]$ can be defined as

$$C \triangleq a[k] = \mathrm{e}^{j\frac{\pi}{4}}, \tag{25}$$

$$x[k] \triangleq f[k] + n'[k], \tag{26}$$

$$y[k] \triangleq \sum_{\nu=1}^{N-1} t_\nu (f[k-\nu] + n'[k-\nu]), \tag{27}$$

with the notation

$$n'[k] \triangleq b^*[k]n[k]. \tag{28}$$

Here, $n'[\cdot]$ is a zero mean white Gaussian random process with variance σ_n^2 like $n[\cdot]$. For the following, the ACF of the process $f[\cdot] + n'[\cdot]$, denoted by $R[\lambda]$, is introduced:

$$R[\lambda] = R_f[\lambda] + \sigma_n^2 \delta[\lambda], \tag{29}$$

where $\delta[\cdot]$ is the unit pulse sequence, i.e., $\delta[0] = 1$, $\delta[\lambda] = 0$, $\lambda \neq 0$. Note, that the process $f[\cdot] + n[\cdot]$ has the same ACF like $f[\cdot] + n'[\cdot]$. If the BER expression of Eq. (4B.21) of [16] is adapted to the problem at hand,

$$P_b = \frac{v_1}{v_1 + v_2} \tag{30}$$

results, with the following definitions:

$$v_1 \triangleq \sqrt{w^2 + \frac{1}{\mu_{xx}\mu_{yy} - |\mu_{xy}|^2}} - w, \tag{31}$$

$$v_2 \triangleq \sqrt{w^2 + \frac{1}{\mu_{xx}\mu_{yy} - |\mu_{xy}|^2}} + w, \tag{32}$$

$$w \triangleq \frac{C\mu_{xy}^* + C^*\mu_{xy}}{2(\mu_{xx}\mu_{yy} - |\mu_{xy}|^2)}, \tag{33}$$

$$\mu_{xx} \triangleq \mathcal{E}\{|x[k]|^2\} = R[0] = \sigma_f^2 + \sigma_n^2, \tag{34}$$

$$\mu_{xy} \triangleq \mathcal{E}\{x[k]y^*[k]\} = \sum_{\nu=1}^{N-1} t_\nu^* R[\nu], \tag{35}$$

$$\mu_{yy} \triangleq \mathcal{E}\{|y[k]|^2\} = \sum_{\nu=1}^{N-1}\sum_{\mu=1}^{N-1} t_\nu t_\mu^* R[\mu - \nu]. \tag{36}$$

Interestingly, the BER for DF–DD of QDPSK depends only on the first N samples $R[0]$, $R[1]$, ..., $R[N-1]$ of the ACF of the process $f[\cdot] + n'[\cdot]$ (cf. Eqs. (34), (35), (36)). For $N = 2$, $t_1 \in \mathbb{R}$, Eq. (30) gives the BER for conventional DD of QDPSK for flat Rayleigh fading (cf. e.g. [17]). Note, that our results for BER are valid for an arbitrary fading spectrum and arbitrary feedback filter (metric) coefficients t_ν, $1 \leq \nu \leq N-1$, i.e., they are also valid for suboptimum coefficients, which are not chosen according to Eq. (15). This will be used in Section 7.

Fig. 4 shows BER vs. $10\log_{10}(E_b/N_0)$ for conventional DD and genie–aided DF–DD of QDPSK for $B_fT = 0.0075$ and $B_fT = 0.03$. Jakes fading model is used (cf. Eq. (19)) and the feedback filter coefficients t_ν, $1 \leq \nu \leq N-1$, are calculated from Eq. (15). It is obvious that an increase of the observation interval NT improves the receiver performance especially at high E_b/N_0 ratios significantly. For $10\log_{10}(E_b/N_0) < 60$ dB there is no error floor if N exceeds 2 and 3 for $B_fT = 0.0075$ and $B_fT = 0.03$, respectively.

5 Relation of DF–DD to Linear Prediction and an Alternative Expression for BER

In this section, we show that the DF–DD receiver for Rayleigh fading contains a linear predictor and we derive an alternative expression for BER. This expression is useful for calculation of the error floor caused by DF–DD and it will be used in the next section to evaluate the limiting performance of our receiver. For derivation of the new expression for BER, we invoke linear prediction theory. First we note, that the coefficients p_ν of a linear FIR predictor of order $N-1$ for the process $f[\cdot]+n'[\cdot]$ can be determined from [13]

$$\boldsymbol{R}\begin{bmatrix} 1 \\ -\boldsymbol{p}^* \end{bmatrix} = \begin{bmatrix} \sigma_e^2 \\ 0 \\ \vdots \\ 0 \end{bmatrix}, \tag{37}$$

where the vector of the prediction filter coefficients is defined as

$$\boldsymbol{p} \stackrel{\triangle}{=} [p_1,\, p_2,\, \ldots,\, p_{N-1}]^T, \tag{38}$$

and σ_e^2 is the variance of the prediction error. Note, that $\boldsymbol{R}$ is defined in Eq. (12). From Eq. (37) it follows, that $t_0 = t_{00}$ and the optimum feedback filter coefficients $t_\nu = t_{0\nu}$, $1 \le \nu \le N-1$, according to Eq. (15) can be expressed by p_ν and σ_e^2:

$$t_0 = -\frac{1}{\sigma_e^2}, \tag{39}$$

$$t_\nu = \frac{p_\nu}{\sigma_e^2}, \qquad 1 \le \nu \le N-1. \tag{40}$$

Using Eq. (40) in addition to the well–known relations [13]

$$\sigma_e^2 = R[0] - \sum_{\nu=1}^{N-1} p_\nu^* R[\nu], \tag{41}$$

$$\sigma_e^2 = R[0] - \sum_{\nu=1}^{N-1}\sum_{\mu=1}^{N-1} p_\nu p_\mu^* R[\mu-\nu], \tag{42}$$

Eqs. (35) and (36) may be rewritten as

$$\mu_{xy} = \frac{\sigma_f^2+\sigma_n^2-\sigma_e^2}{\sigma_e^2}, \tag{43}$$

$$\mu_{yy} = \frac{\sigma_f^2+\sigma_n^2-\sigma_e^2}{\sigma_e^4}. \tag{44}$$

By applying Eqs. (34), (43) and (44) to Eqs. (31) – (33), Eq. (30) can be simplified to

$$P_b = \frac{1}{2}\left(1 - \sqrt{\frac{\sigma_f^2 + \sigma_n^2 - \sigma_e^2}{\sigma_f^2 + \sigma_n^2 + \sigma_e^2}}\right), \tag{45}$$

i.e., BER depends exclusively on σ_f^2, σ_n^2 and the prediction–error variance σ_e^2 caused by the $(N-1)$st order predictor for the process $f[\cdot] + n'[\cdot]$.

Eq. (45) clearly shows that $P_b > 0$ for $\sigma_e^2 > 0$ even in the absence of noise ($\sigma_n^2 = 0$), i.e., in this case there is an irreducible error floor. From Eqs. (37), (41) and (42) it can be seen that σ_e^2 depends only on the first N samples of the fading ACF if $\sigma_n^2 = 0$. Thus, because of Eq. (45), the error floor caused by DF–DD also depends only on the first N samples of the fading ACF. For $\sigma_n^2 = 0$, Figs. 5a) and 5b) show, respectively, σ_e^2 and BER vs. N for $B_f T = 0.0075$ and $B_f T = 0.03$. Again, Jakes fading model is used. Note, that for the special case $N = 1$, the results $\sigma_e^2 = \sigma_f^2$ ($= 1$ because of normalization) and $P_b = \frac{1}{2}$ are obtained immediately. Both, σ_e^2 and P_b decrease with increasing N. Note, that for a given N the error floor of the proposed DF–DD receiver for MDPSK is lower for the smaller fading bandwidth.

The feedback filter coefficients t_ν, $1 \leq \nu \leq N-1$, are essentially equal to the linear predictor coefficients for the process $f[\cdot] + n'[\cdot]$ (cf. Eq. (40)). A prediction–based coherent receiver with similar coefficients has been proposed for QDPSK [20] by Svensson. The scheme in [20] is only formulated for $M = 4$ but could also be extended to $M \neq 4$. However, corresponding to the principle of coherent detection the receiver in [20] determines an estimate $\hat{b}[k]$ for the MPSK symbol $b[k]$ and then calculates $\hat{a}[k]$ by inverting differential encoding ($\hat{a}[k] = \hat{b}[k]\hat{b}^*[k-1]$). Corresponding to the principle of noncoherent (differential) detection the DF–DD receiver proposed here directly estimates the MDPSK symbol $a[k]$. In [20], MPSK decision–feedback symbols $\hat{b}[\cdot]$ are used instead of MDPSK decision–feedback symbols $\hat{a}[\cdot]$. Moreover, it is mentioned in [20] that initially at least one known symbol has to be transmitted. This is not necessary here, since our feedback filter only needs MDPSK symbols and thus, for detection of the first $N-1$ symbols a conventional differential detector could be used. Finally, the resulting filter in [20] is time–variant, whereas the DF–DD feedback filter is time–invariant.

In the DF–DD scheme for AWGN channels the FIR feedback filter might be replaced by a one–tap IIR feedback filter [21]. Motivated by this, for Rayleigh fading we could also replace the FIR feedback filter by an IIR filter, i.e., essentially an IIR predictor for

the process $f[\cdot]+n'[\cdot]$ would have to be designed. However, an IIR predictor only offers an advantage if a moving average (MA) model of the process $f[\cdot]+n'[\cdot]$ requires less parameters than an autoregressive (AR) model [22]. Since for all commonly used fading models $f[\cdot]+n'[\cdot]$ is well approximated by an AR model of low order, we do not consider IIR predictors here. The efficiency of FIR predictors for the problem at hand is also confirmed by Fig. 5a). Note, that even a first order FIR predictor ($N=2$) reduces σ_e^2 approximately by a factor of 50 and 1000 for $B_fT=0.03$ and $B_fT=0.0075$, respectively.

Hamamoto showed in [23] that a one–tap IIR feedback filter designed for the AWGN case also provides a gain over conventional DD for Ricean fading if the filter coefficient α is optimized. However, the results presented in [23] confirm that for Rayleigh fading (i.e., the Ricean factor is zero) $\alpha=0$ (corresponding to conventional DD) is optimum, i.e., in this case a one–tap IIR filter cannot improve conventional DD.

6 Performance in the Limit $N\to\infty$

Now, we evaluate the limiting performance of DF-DD with error–free feedback for $N\to\infty$. Although such a receiver is not implementable, of course, it is interesting to know the fundamental limits of DF–DD and how these limits depend on parameters of the underlying fading process.

From Eq. (45) it can be seen that P_b becomes minimum for minimum $\sigma_e^2\geq 0$. The minimum prediction–error variance $\sigma_{e,\min}^2$ is obtained for $N\to\infty$ and given by [24, 25]:

$$\sigma_{e,\min}^2=\exp\left(T\int\limits_{-1/(2T)}^{1/(2T)}\log\left(S(\mathrm{e}^{j2\pi fT})\right)\,\mathrm{d}f\right), \tag{46}$$

where the power spectral density $S(\mathrm{e}^{j2\pi fT})$ is the Fourier transform of the ACF $R[\lambda]$ (cf. Eq. (29)). Thus, $S(\mathrm{e}^{j2\pi fT})$ can be expressed as

$$S(\mathrm{e}^{j2\pi fT})=S_f(\mathrm{e}^{j2\pi fT})+\sigma_n^2, \tag{47}$$

where $S_f(\mathrm{e}^{j2\pi fT})$ denotes the power spectral density of the fading process.

In the sequel, we consider three special cases of Eqs. (45) and (46).

A. $\sigma_n^2=0$

In this case, $\sigma_{e,\min}^2$ and P_b depend exclusively on the fading spectrum. According

to [24, 25], $\sigma^2_{e,\min}$ is equal to zero if $S_f(\mathrm{e}^{j2\pi fT})$ is zero over a noncountable set of frequencies (i.e., over a line segment). Then, $P_b = 0$ follows from Eq. (45). This means, for ideally bandlimited fading spectra (e.g. Jakes spectrum) there is no irreducible error floor. Note, that a similar result is reported in [26] for continuous phase modulation (CPM).

B. $B_f \to 0$

If the fading bandwidth B_f approaches zero, $R_f[\lambda]$ is constant $\forall\, \lambda$ and $S_f(\mathrm{e}^{j2\pi fT})$ is given by

$$S_f(\mathrm{e}^{j2\pi fT}) = \sigma_f^2\, \delta_0(f), \qquad |f| \leq 1/(2T), \tag{48}$$

where $\delta_0(\cdot)$ is the Dirac delta function [27]. In Appendix A, we demonstrate that in this case $\sigma^2_{e,\min}$ is equal to σ_n^2. Thus, P_b is given by

$$P_b = \frac{1}{2}\left(1 - \frac{1}{\sqrt{1 + 2\frac{\sigma_n^2}{\sigma_f^2}}}\right). \tag{49}$$

This is exactly the same BER as obtained for coherent QPSK with perfect channel state information [16]. This result is in perfect accordance with [2], where it was shown that for the AWGN channel genie–aided DF–DD for $N \to \infty$ yields the same BER as coherent PSK, too. Note, that the BER of QDPSK with genie–aided DF–DD is lower than that of QDPSK with coherent detection with perfect channel state information. This is because error propagation is avoided by the genie.

C. Jakes Fading Model

To become more specific, we assume the widely used fading model of Jakes [14]:

$$S_f(\mathrm{e}^{j2\pi fT}) = \begin{cases} \frac{\sigma_f^2}{\pi T\sqrt{B_f^2 - f^2}} & |f| < B_f \\ 0 & B_f \leq |f| \leq \frac{1}{2T} \end{cases}, \tag{50}$$

where $S_f(\mathrm{e}^{j2\pi fT})$ is the Fourier transform of $R_f[\lambda]$ according to Eq. (19). It can be shown (cf. Appendix B) that in this special case $\sigma^2_{e,\min}$ is given by

$$\sigma^2_{e,\min} = \sigma_n^2 \left(\frac{\mathrm{e}\sigma_f^2}{2\pi B_f T \sigma_n^2}\right)^{2B_fT} \exp(2T I_2), \tag{51}$$

where e is the Euler number [27] and the constant I_2 is defined in Appendix B. As was to be expected from Case B., for $B_f \to 0$ $\sigma^2_{e,\min}$ approaches σ_n^2 (cf. Eqs. (51), (60)).

Fig. 6 shows BER vs. $10\log_{10}(E_b/N_0)$ for QDPSK and different values of B_fT. As can be seen, for $B_fT = 0$ genie–aided DF–DD performs as good as coherent QPSK with perfect channel state information. As B_fT grows, BER increases and the slope of the curves decreases. This clearly shows, that for $B_fT > 0$ a performance loss is unavoidable in comparison to $B_fT = 0$ even for $N \to \infty$. Since $S_f(\mathrm{e}^{j2\pi fT})$ is strictly bandlimited (cf. Eq. (50)), no error floor can be observed as was to be expected from Case A.

7 Simulation Results

For all simulation results presented in this section a QDPSK ($M = 4$) constellation is assumed. Although the fading simulation program used here is based on Jakes model, the generated fading process cannot be bandlimited. This is illustrated in Figs. 7a) and 7b) for $B_fT = 0.0075$ and $B_fT = 0.03$, respectively. Like for any realizable fading process the power spectral density of the simulated fading process does not vanish identically for $B_f \leq |f| \leq 1/(2T)$. This means, in contrast to the theoretical model there is an irreducible error floor even for $N \to \infty$. For $\sigma_n^2 = 0$, $\sigma^2_{e,\min}$ for the simulated fading processes can be determined from the spectra of Figs. 7a) and 7b) according to Eq. (46) using numerical integration. The resulting irreducible error floor (cf. Eq. (45)) for genie–aided DF–DD is $P_b = 3.12 \cdot 10^{-5}$ and $P_b = 0.94 \cdot 10^{-5}$ for $B_fT = 0.0075$ and $B_fT = 0.03$, respectively.

In the sequel, for metric and BER calculations autocorrelation estimates $\hat{R}_f[\lambda]$, $0 \leq \lambda \leq N-1$, determined from samples of the simulated fading process, are used. In practice, the fading process is not known at the receiver. However, this is not a major problem since $R[\lambda]$, $0 \leq \lambda \leq N-1$, can be directly estimated using the remodulated received signal samples $r[\cdot]b^*[\cdot]$. For remodulation, either known pilot symbols $b[\cdot]$ or decision feedback symbols $\hat{b}[\cdot]$ can be used.

Fig. 8 shows the BER vs. $10\log_{10}(E_b/N_0)$ for MSD, DF–DD and genie–aided DF–DD for $N = 2$, 3, 4 and $B_fT = 0.0075$ ($\hat{R}_f[0] = 1.0$, $\hat{R}_f[1] = 0.9994$, $\hat{R}_f[2] = 0.9979$, $\hat{R}_f[3] = 0.9953$). The metric coefficients $t_{\nu\,\mu}$, $0 \leq \nu, \mu \leq N-1$, are determined from Eq. (15). For comparison the BER for coherent detection (CD) of QDPSK with perfect channel state information is given, too, because it represents a lower bound for (realizable) noncoherent

detection schemes. It can be seen that the error floor for conventional DD ($N = 2$) is reduced by both MSD and DF–DD for $N = 3$ and $N = 4$. DF–DD performs as good as MSD, whereas genie–aided DF–DD even outperforms MSD. Obviously, the simulated and calculated (denoted by 'Theory') BERs for genie–aided DF–DD and conventional DD are in good agreement. Feeding back previously decided symbols instead of error–free symbols causes an increase of the BER by approximately a factor of two. At low E_b/N_0 ratios, conventional DD performs almost as good as CD and no gain can be obtained by enlargement of the observation interval N.

Fig. 9 compares genie–aided DF–DD using optimum and suboptimum feedback filter (metric) coefficients t_ν for $B_fT = 0.03$ ($\hat{R}_f[0] = 1.0$, $\hat{R}_f[1] = 0.9917$, $\hat{R}_f[2] = 0.9671$, $\hat{R}_f[3] = 0.9267$). If the suboptimum AWGN feedback filter (metric) coefficients, i.e., t_ν = const., $1 \leq \nu \leq N-1$, are used, the error floor increases with increasing N, whereas it decreases significantly when the optimum feedback filter (metric) coefficients according to Eq. (15) are applied. Here, for DF–DD ($N = 3$ and $N = 4$) with optimum feedback filter (metric) coefficients the error floor is about 40 times lower than for conventional DD ($N = 2$).

8 Conclusions

DF–DD of MDPSK signals transmitted over flat Rayleigh fading channels has been introduced in this paper. The simple DF–DD decision rule has been derived from the optimum MSD metric and it has been shown that the feedback filter is related to a linear Wiener predictor. For genie–aided DF–DD, the exact BER for QDPSK transmission has been calculated and it has been demonstrated that BER depends only on the variance of the fading process, the variance of the noise process and the prediction–error variance. If B_f approaches zero, QDPSK with genie–aided DF–DD has the same BER like coherent QPSK if feedback filters of infinite order are applied. Furthermore, it has also been shown that the error floor (i.e., BER for $\sigma_n^2 = 0$) caused by DF–DD depends exclusively on the first N samples of the ACF of the fading process; for $N \to \infty$ a direct relation to the fading spectrum exists. For ideally bandlimited fading processes the error floor of conventional DD can be removed entirely if a feedback filter of infinite order is applied. Simulations show that both, MSD and DF–DD with feedback filters of finite order can reduce the

error floor caused by conventional DD significantly. While, in principle, complexity of MSD grows exponentially with increasing observation interval NT, it only grows linearly for DF–DD.

Acknowledgement

The authors would like to thank TCMC (Technology Centre for Mobile Communication), Philips Semiconductors, Germany, for supporting this work.

References

[1] H. Leib, S. Pasupathy: The Phase of a Vector Perturbed by Gaussian Noise and Differentially Coherent Receivers, *IEEE Trans. on Information Theory*, Vol. 34, No. 6, Nov. 1988, pp. 1491 - 1501.

[2] F. Edbauer: Bit Error Rate of Binary and Quaternary DPSK Signals with Multiple Differential Feedback Detection, *IEEE Trans. on Commun.*, Vol. 40, No. 3, Mar. 1992, pp. 457 - 460.

[3] P. A. Bello, B. D. Nelin: The Influence of Fading Spectrum on the Binary Error Probabilities of Incoherent and Differentially Coherent Matched Filter Receivers, *IRE Trans. on Commun. Sys.*, Vol. CS–10, Jun. 1962, pp. 160 -168.

[4] D. Divsalar, M. K. Simon: Multiple-Symbol Differential Detection of MPSK, *IEEE Trans. on Commun.*, Vol. 38, No. 3, Mar. 1990, pp. 300 - 308.

[5] D. Divsalar, M. K. Simon: Maximum–Likelihood Differential Detection of Uncoded and Trellis Coded Amplitude Phase Modulation over AWGN and Fading Channels — Metrics and Performance, *IEEE Trans. on Commun.*, Vol. 42, No. 1, Jan. 1994, pp. 76 - 89.

[6] P. Ho, D. Fung: Error Performance of Multiple–Symbol Differential Detection of PSK Signals Transmitted Over Correlated Rayleigh Fading Channels, *IEEE Trans. on Commun.*, Vol. 40, No. 10, Oct. 1992, pp. 25 - 29.

[7] F. Adachi, M. Sawahashi: Decision Feedback Multiple–Symbol Differential Detection for M–ary DPSK, *Electronics Letters*, Vol. 29, No. 15, Jul. 1993, pp. 1385 - 1387.

[8] G. M. Vitetta, D. P. Taylor: Viterbi Decoding of Differentially Encoded PSK Signals Transmitted over Rayleigh Frequency–Flat Fading Channels, *IEEE Trans. on Commun.*, Vol. 43, No. 2/3/4, Feb.-Apr. 1995, pp. 1256 - 1259.

[9] X. Yu, S. Pasupathy: Innovations–Based MLSE for Rayleigh Fading Channels, *IEEE Trans. on Commun.*, Vol. 43, No. 2/3/4, Feb.-Apr. 1995, pp. 1534 - 1544.

[10] W. C. Dam, D. P. Taylor: An Adaptive Maximum Likelihood Receiver for Correlated Rayleigh–Fading Channels, *IEEE Trans. on Commun.*, Vol. 42, No. 9, Sep. 1994, pp. 2684 - 2692.

[11] D. Makrakis, P. T. Mathiopoulos, D. P. Bouras: Optimal Decoding of Coded PSK and QAM Signals in Correlated Fast Fading Channels and AWGN: A Combined Envelope, Multiple Differential and Coherent Detection Approach, *IEEE Trans. on Commun.*, Vol. 42, No. 1, Jan. 1994, pp. 63 - 74.

[12] K. Miller: *Complex Stochastic Processes*, Addison–Wesley, New York, 1974.

[13] S. Haykin: *Adaptive Filter Theory*, 3rd edition, Prentice Hall, New Jersey, 1996.

[14] W. C. Jakes, Jr., Ed.: *Microwave Mobile Communications*, Wiley, New York, 1974.

[15] T. S. Rappaport: *Wireless Communications*, Prentice Hall, New Jersey, 1996.

[16] J. G. Proakis: *Digital Communications*, 2nd edition, McGraw-Hill, New York, 1989.

[17] A. Neul: Bit error rate for 4–DPSK in fast Ricean fading and Gaussian noise, *IEEE Trans. on Commun.*, Vol. 37, No. 12, Dec. 1989, pp. 1385 - 1387.

[18] K. M. Mackenthun, Jr.: A Fast Algorithm for Multiple–Symbol Differential Detection of MPSK, *IEEE Trans. on Commun.*, Vol. 42, No. 2/3/4, Feb.-Apr. 1994, pp. 1471 - 1474.

[19] M. K. Simon, S. M. Hinedi, W. C. Lindsey: *Digital Communication Techniques: Signal Design and Detection*, Prentice–Hall, New Jersey, 1994.

[20] A. Svensson: Coherent detector based on linear prediction and decision feedback for DQPSK, *Electronics Letters*, Vol. 30, No. 20, Sep. 1994, pp. 1642 - 1643.

[21] H. Leib: Data–Aided Noncoherent Demodulation of DPSK, *IEEE Trans. on Commun.*, Vol. 43, No. 2/3/4, Feb.-Apr., 1995, pp. 722 - 725.

[22] S. M. Kay: *Modern Spectral Estimation: Theory and Application*, Prentice–Hall, New Jersey, 1988.

[23] N. Hamamoto: Differential Detection with IIR Filter for Improving DPSK Detection Performance, *IEEE Trans. on Commun.*, Vol. 44, No. 8, Aug. 1996, pp. 959 - 966.

[24] J. Makhoul: Linear Prediction: A Tutorial Review, *Proceedings of the IEEE*, Vol. 63, No. 4, Apr. 1975, pp. 561 - 580.

[25] M. B. Priestley: *Spectral Analysis and Time Series, Volume 2: Multivariate Series, Prediction and Control*, Academic Press, Inc., Orlando, Florida, 1981.

[26] J. H. Lodge, M. L. Moher: Maximum Likelihood Sequence Estimation of CPM Signals Transmitted Over Rayleigh Flat–Fading Channels, *IEEE Trans. on Commun.*, Vol. 38, No. 6, Jun. 1990, pp. 787 - 794.

[27] E. J. Borowski, J. M.Borwein: *The Harper Collins Dictionary of Mathematics*, Harper Perennial, New York, 1991.

[28] I. S. Gradshteyn, I. M .Ryzhik: *Table of Integrals, Series, and Products*, Academic Press, New York, 1965.

Appendix A

In order to prove $\sigma^2_{e,\min} = \sigma^2_n$ for $B_f \to 0$, we approximate $S_f(\mathrm{e}^{j2\pi fT})$ (cf. Eq. (48)) by

$$S_f(\mathrm{e}^{j2\pi fT}) = \lim_{B_f \to 0} u_{B_f}(\mathrm{e}^{j2\pi fT}), \tag{52}$$

with

$$u_{B_f}(\mathrm{e}^{j2\pi fT}) = \begin{cases} \frac{\sigma_f^2}{2B_fT} & |f| < B_f \\ 0 & B_f \le |f| \le \frac{1}{2T} \end{cases} . \tag{53}$$

Using this and the symmetry of $S(\mathrm{e}^{j2\pi fT})$ (cf. Eqs. (47), (53)), $\sigma^2_{e,\min}$ from Eq. (46) can be rewritten to

$$\begin{aligned} \sigma^2_{e,\min} &= \lim_{B_f \to 0} \left\{ \exp\left(2T \left(\int_0^{B_f} \log\left(\frac{\sigma_f^2}{2B_fT} + \sigma_n^2 \right) \mathrm{d}f + \int_{B_f}^{1/(2T)} \log(\sigma_n^2)\, \mathrm{d}f \right) \right) \right\} \\ &= \lim_{B_f \to 0} \left\{ \exp\left(2B_fT \log\left(\frac{\sigma_f^2}{2B_fT} + \sigma_n^2 \right) + (1 - 2B_fT) \log(\sigma_n^2) \right) \right\} \\ &= \sigma_n^2, \end{aligned} \tag{54}$$

which is the expected result.

Appendix B

In this appendix, $\sigma^2_{e,\min}$ is calculated for Jakes fading spectrum. Because of the symmetry of $S(\mathrm{e}^{j2\pi fT})$ (cf. Eqs. (47), (50)), Eq. (46) may be rewritten to

$$\begin{aligned}\sigma^2_{e,\min} &= \exp\left(2T\left(\int_0^{B_f}\log\left(\frac{\sigma_f^2}{\pi B_f T\sqrt{1-\left(\frac{f}{B_f}\right)^2}}+\sigma_n^2\right)\mathrm{d}f+\int_{B_f}^{1/(2T)}\log\left(\sigma_n^2\right)\mathrm{d}f\right)\right)\\ &= \exp\left(2T\left(\underbrace{\int_0^{B_f}\log\left(\frac{q_1}{\sqrt{1-\left(\frac{f}{B_f}\right)^2}}\right)\mathrm{d}f}_{\triangleq I_1}+\underbrace{\int_0^{B_f}\log\left(1+q_2\sqrt{1-\left(\frac{f}{B_f}\right)^2}\right)\mathrm{d}f}_{\triangleq I_2}\right)\right)\\ &\quad\cdot(\sigma_n^2)^{1-2B_fT},\end{aligned}\tag{55}$$

where the definitions $q_1=\frac{\sigma_f^2}{\pi B_f T}$ and $q_2=\frac{\pi B_f T\sigma_n^2}{\sigma_f^2}$ are used.

I_1 can be evaluated by using the substitution $\cos\varphi=\frac{f}{B_f}$; this leads to

$$I_1=B_f\left(\int_0^{\pi/2}\log(q_1)\sin\varphi\,\mathrm{d}\varphi-\int_0^{\pi/2}\log(\sin\varphi)\sin\varphi\,\mathrm{d}\varphi\right).\tag{56}$$

Using the identity $\int_0^{\pi/2}\log(\sin\varphi)\sin\varphi\,\mathrm{d}\varphi=\log(2)-1$ [28] we get

$$I_1=B_f\log\left(\frac{\mathrm{e}}{2}q_1\right),\tag{57}$$

where e is the Euler number [27]. For the calculation of I_2 the substitution $\cos\varphi=\frac{f}{B_f}$ is applied, too:

$$I_2=B_f\int_0^{\pi/2}\log(1+q_2\sin\varphi)\sin\varphi\,\mathrm{d}\varphi.\tag{58}$$

In the following, we assume $q_2<1$. This is not a strong restriction as long as B_fT is small. Here, we assume $B_fT\le 0.03$, i.e., $q_2<1$ requires $\sigma_n^2/\sigma_f^2<100/(3\pi)$. This means for QDPSK ($M=4$, $\sigma_n^2=\frac{N_0}{2E_b}$) our assumption is justified for $10\log_{10}(E_b/N_0)>-13.3$ dB. Now the logarithm in Eq. (58) can be replaced by its Taylor series [28]:

$$I_2 = B_f\int_0^{\pi/2}\sum_{\nu=1}^{\infty}(-1)^{\nu+1}\frac{q_2^\nu}{\nu}(\sin\varphi)^{\nu+1}\mathrm{d}\varphi$$

$$= \quad -B_f \sum_{\nu=1}^{\infty} \frac{(-q_2)^\nu}{\nu} \int_0^{\pi/2} (\sin\varphi)^{\nu+1} \mathrm{d}\varphi. \tag{59}$$

Applying $\int_0^{\pi/2} (\sin x)^{\mu-1} \mathrm{d}x = 2^{\mu-2}\mathrm{B}(\frac{\mu}{2}, \frac{\mu}{2})$, $\mu \in \mathbb{Z}$, $\mu > 0$ [28], where $\mathrm{B}(\cdot,\cdot)$ is the Beta function, Eq. (59) yields

$$I_2 = -B_f \sum_{\nu=1}^{\infty} \frac{(-q_2)^\nu}{\nu} 2^\nu \mathrm{B}\left(\frac{\nu}{2}+1, \frac{\nu}{2}+1\right). \tag{60}$$

By inserting I_1 of Eq. (57) and I_2 into Eq. (55), Eq. (51) can be obtained.

Figure Captions:

Figure 1: Block diagram of the transmission model.

Figure 2: Normalized metric coefficients $p_\nu = \sigma_e^2 t_\nu$ vs. $10\log_{10}(E_b/N_0)$ for a QDPSK constellation ($M = 4$) for Jakes fading model with normalized fading bandwidths a) $B_fT = 0.0075$; b) $B_fT = 0$.

Figure 3: Structure of the DF–DD receiver.

Figure 4: BER of QDPSK vs. $10\log_{10}(E_b/N_0)$ for conventional DD ($N = 2$) and genie–aided DF–DD ($N = 3$, 4) for Jakes fading model ($B_fT = 0.0075$ and $B_fT = 0.03$).

Figure 5: a) Prediction–error variance σ_e^2 vs. the number of observation intervals N for genie–aided DF–DD; b) BER for $\sigma_n^2 = 0$ (error floor) of QDPSK vs. N for genie–aided DF–DD.

Figure 6: BER vs. $10\log_{10}(E_b/N_0)$ for QPSK with coherent detection and QDPSK with genie–aided DF–DD ($N \to \infty$) for different fading bandwidths B_f. Jakes fading model is assumed.

Figure 7: Theoretical and simulated Jakes fading spectrum with bandwidths a) $B_fT = 0.0075$; b) $B_fT = 0.03$.

Figure 8: BER of QDPSK vs. $10\log_{10}(E_b/N_0)$ for conventional DD ($N = 2$), DF–DD, genie–aided DF–DD, MSD, and coherent detection (CD) with perfect channel state information for $B_fT = 0.0075$.

Figure 9: BER of QDPSK vs. $10\log_{10}(E_b/N_0)$ for conventional DD ($N = 2$), DF–DD (optimum feedback filter (metric) coefficients), genie–aided DF–DD (optimum and AWGN feedback filter (metric) coefficients), and CD with perfect channel state information for $B_fT = 0.03$.

Figures:

Figure 1:

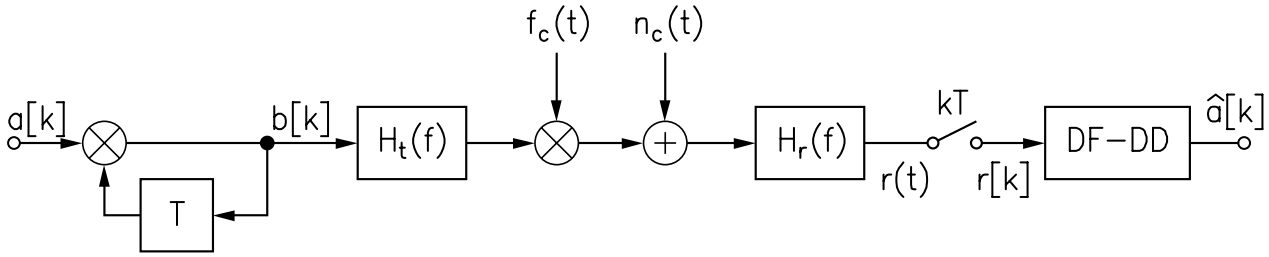

Figure 2:

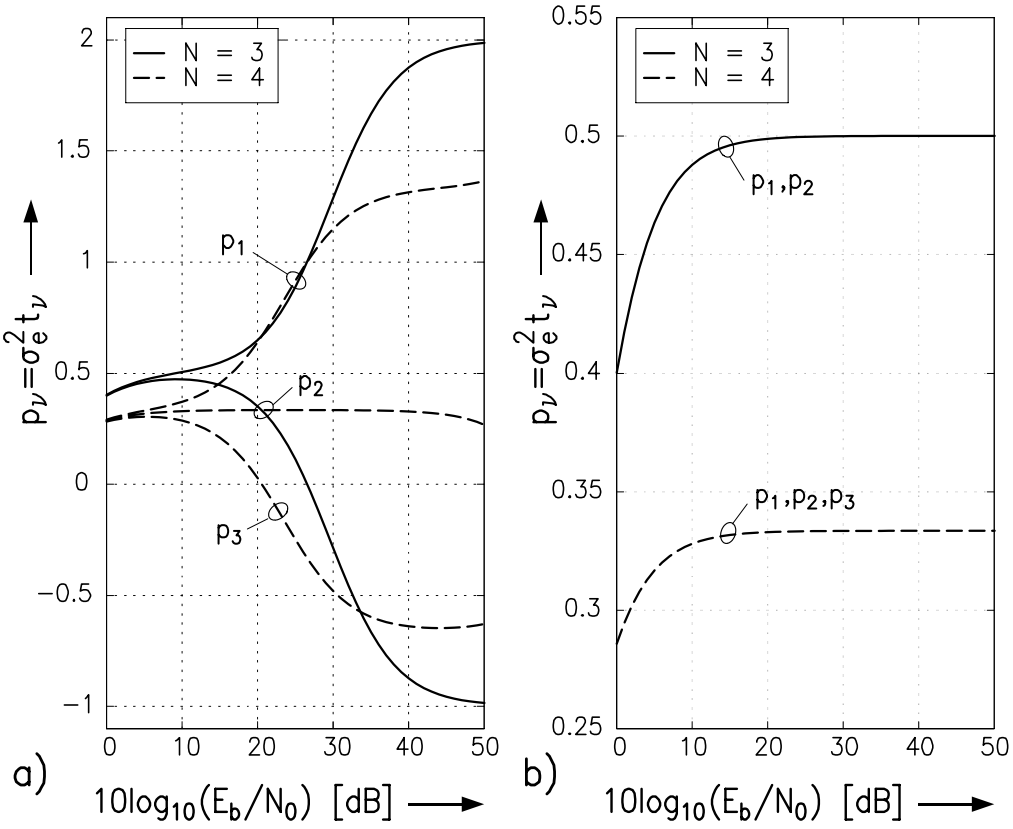

Figure 3:

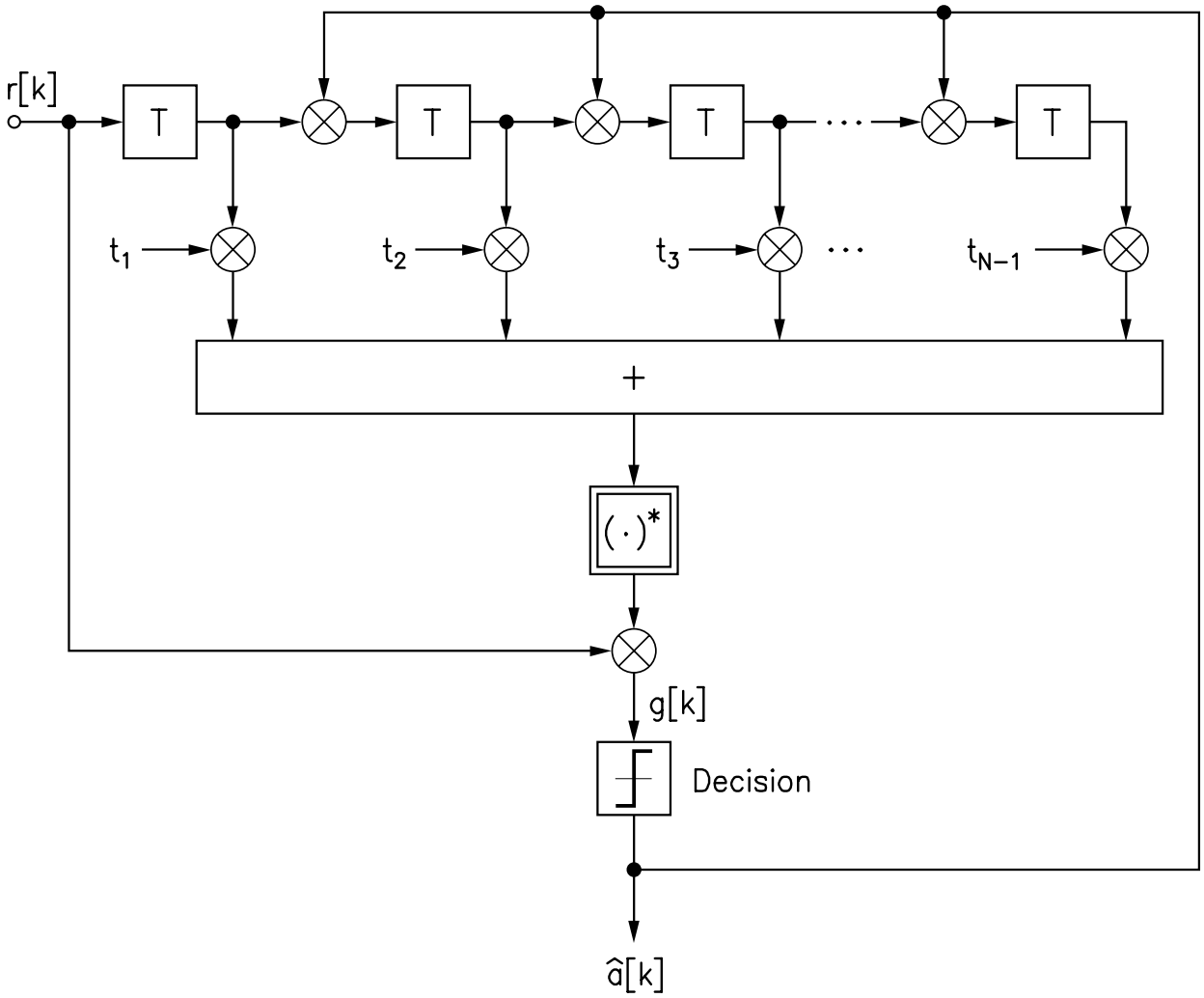

Figure 4:

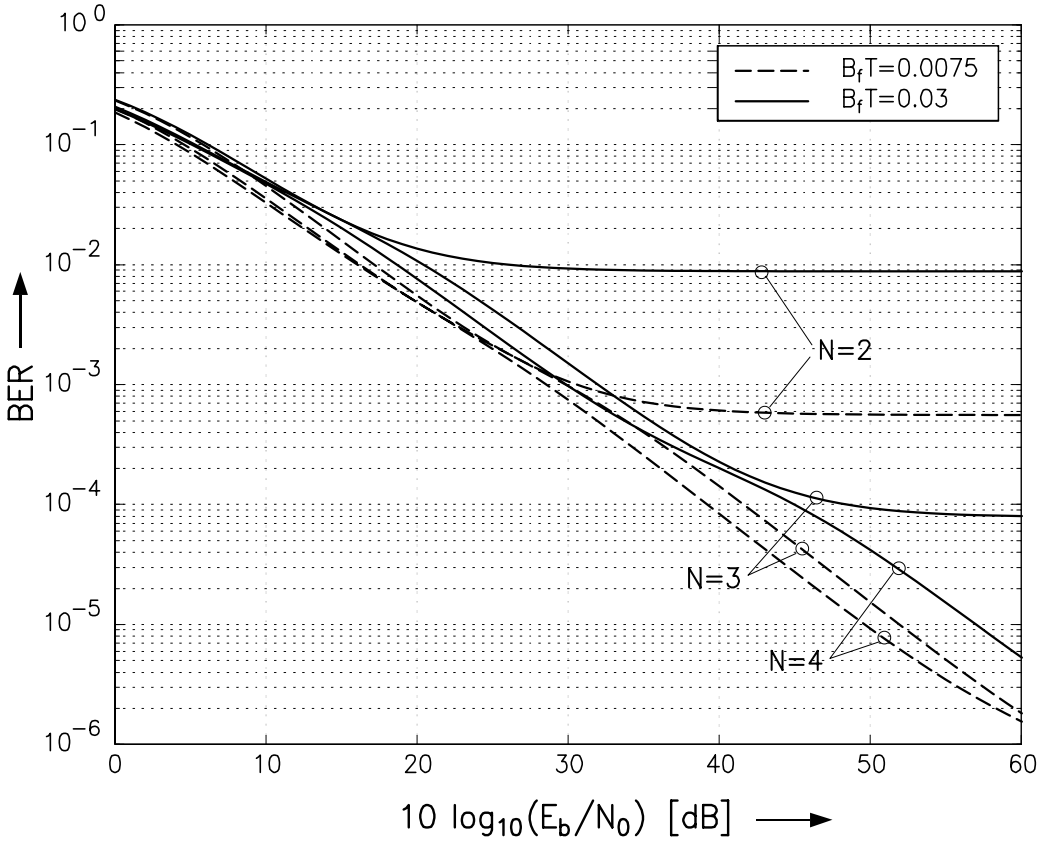
10^0
10^{-1}
10^{-2}
10^{-3}
10^{-4}
10^{-5}
10^{-6}
BER
0
10
20
30
40
50
60
10 $\log_{10}(E_b/N_0)$ [dB]
B_fT=0.0075
B_fT=0.03
N=2
N=3
N=4

Figure 5:

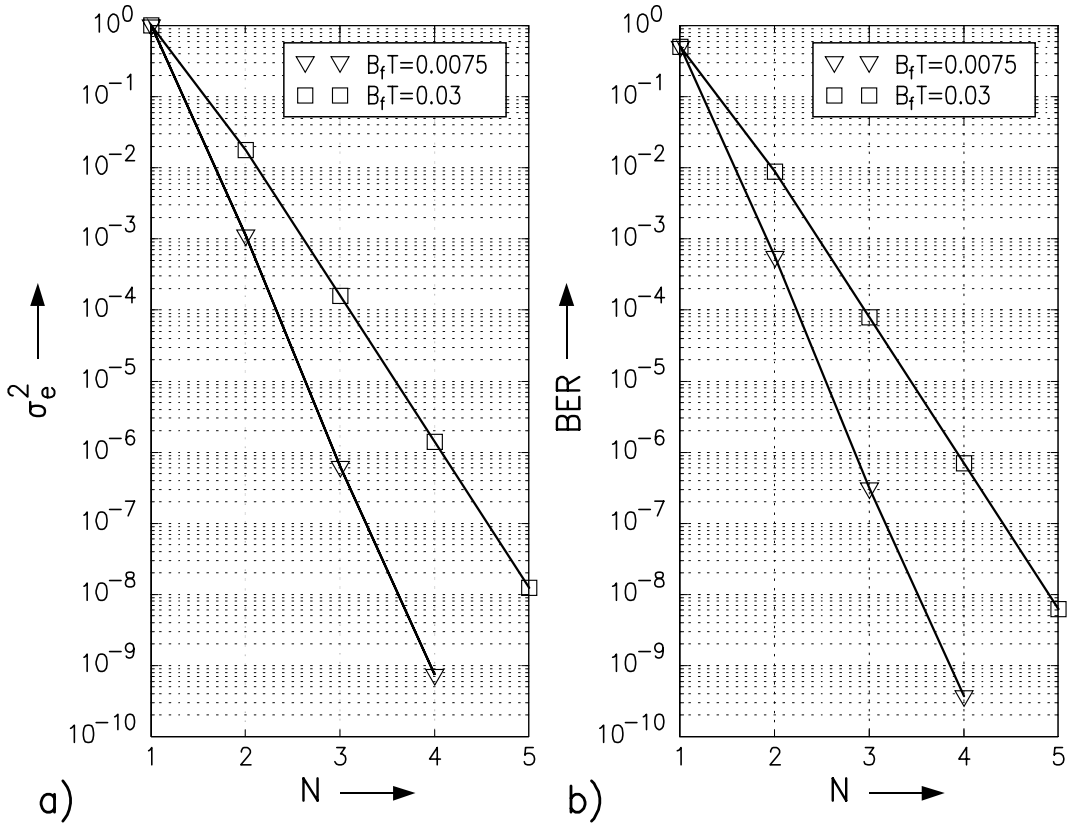
10^0
10^{-1}
10^{-2}
10^{-3}
10^{-4}
10^{-5}
10^{-6}
10^{-7}
10^{-8}
10^{-9}
10^{-10}
σ_e^2
BER
1
2
3
4
5
N
B_fT=0.0075
B_fT=0.03
a)
b)

Figure 6:

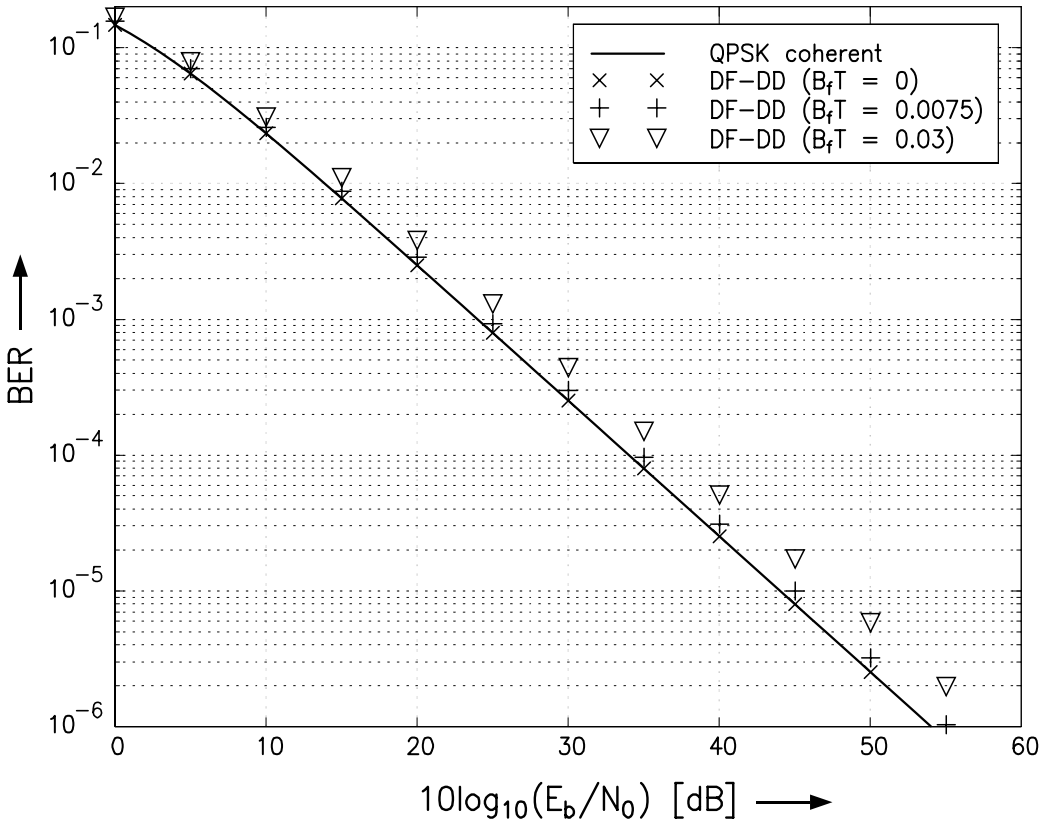
QPSK coherent
DF–DD (B_fT = 0)
DF–DD (B_fT = 0.0075)
DF–DD (B_fT = 0.03)
BER
10^{-1}
10^{-2}
10^{-3}
10^{-4}
10^{-5}
10^{-6}
0
10
20
30
40
50
60
$10\log_{10}(E_b/N_0)$ [dB]

Figure 7:

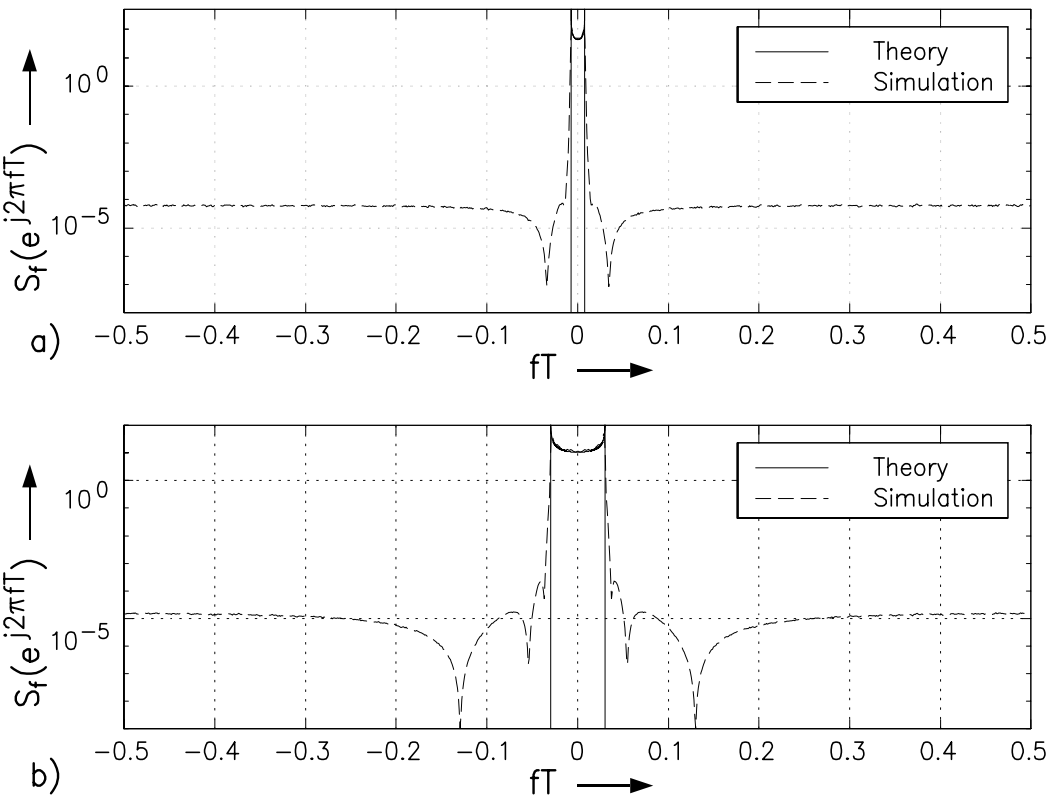
Theory
Simulation
10^0
10^{-5}
$S_f(e^{j2\pi fT})$
a)
−0.5 −0.4 −0.3 −0.2 −0.1 0 0.1 0.2 0.3 0.4 0.5
fT
Theory
Simulation
10^0
10^{-5}
$S_f(e^{j2\pi fT})$
b)
−0.5 −0.4 −0.3 −0.2 −0.1 0 0.1 0.2 0.3 0.4 0.5
fT

Figure 8:

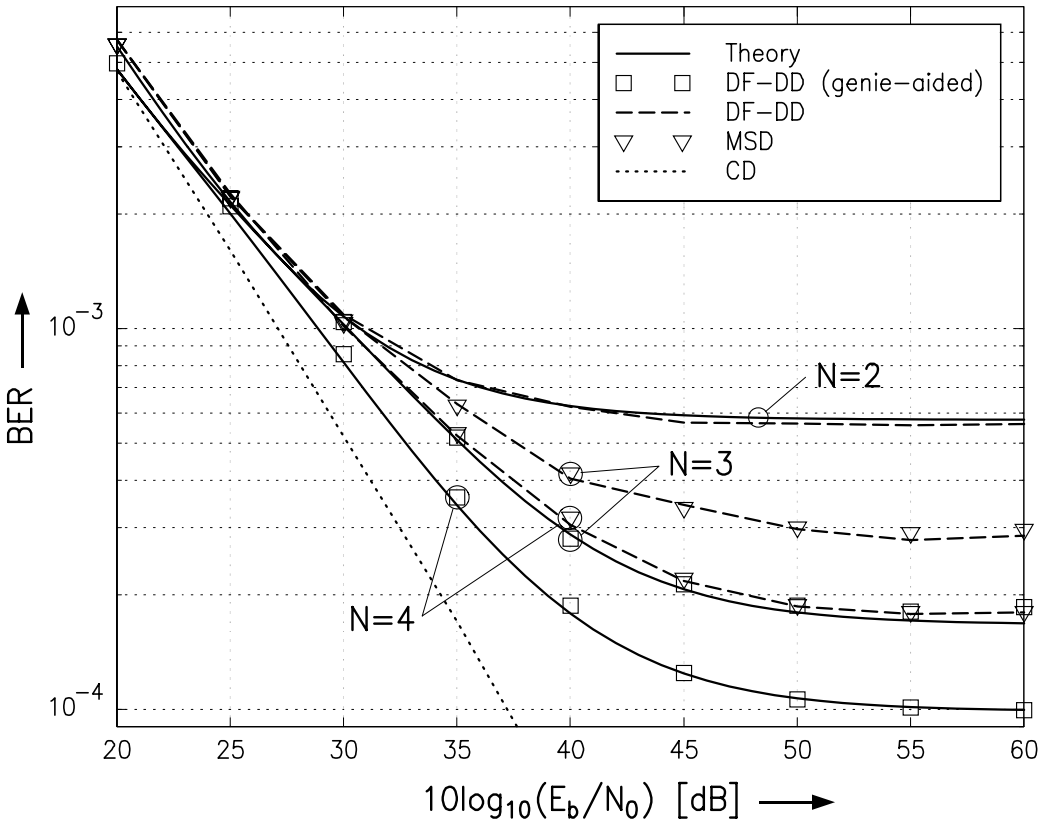
Theory
DF–DD (genie–aided)
DF–DD
MSD
CD
BER
10^{-3}
10^{-4}
N=2
N=3
N=4
20
25
30
35
40
45
50
55
60
$10\log_{10}(E_b/N_0)$ [dB]

Figure 9:

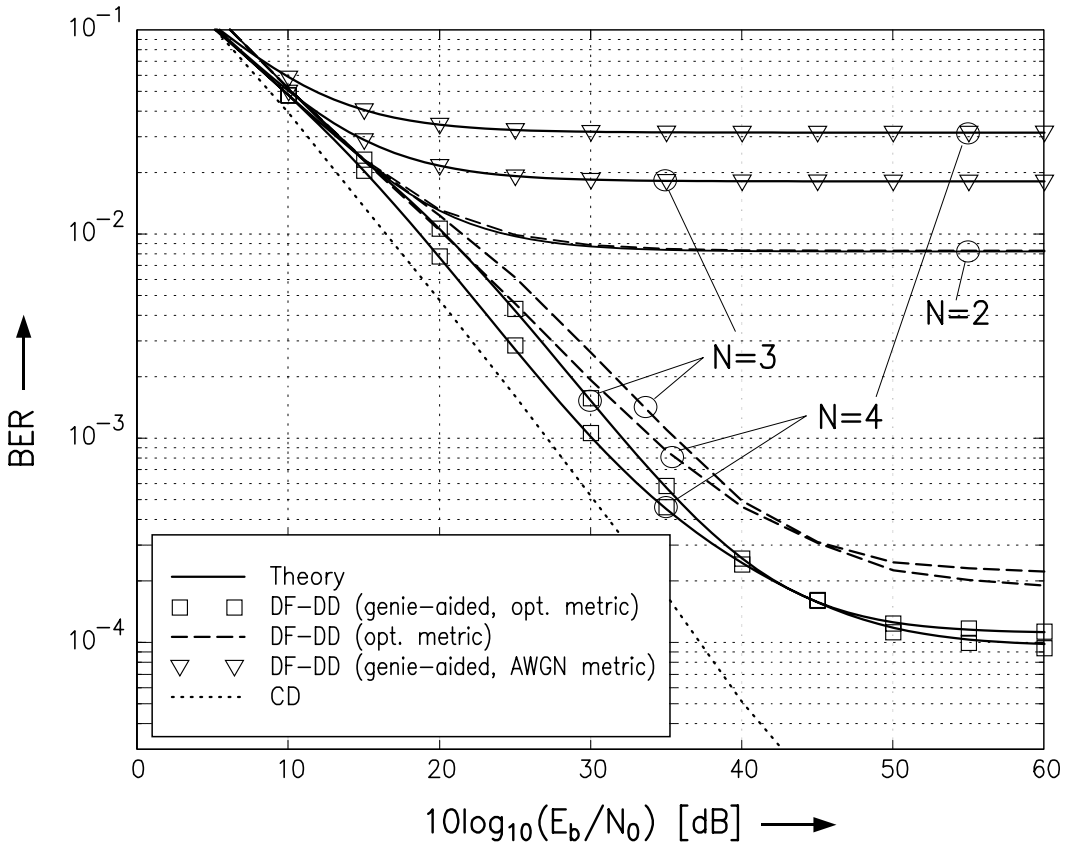
BER
10^{-1}
10^{-2}
10^{-3}
10^{-4}
0
10
20
30
40
50
60
$10\log_{10}(E_b/N_0)$ [dB]
N=2
N=3
N=4
Theory
DF–DD (genie–aided, opt. metric)
DF–DD (opt. metric)
DF–DD (genie–aided, AWGN metric)
CD